High Speed Camera System for BNL E951 Muon Targetry Experiment

December 15, 2000
on Targetry R&D Meeting at BNL

Haipeng Wang, Thomas Tsang
Brookhaven National Lab

Outlines:

1. The first order (conceptual optics) design has been done by Kirk McDonald. Critical components have been purchased. The second order (engineering details) design is in progress.

2. Bench tests for the camera image capture speed have been done at BNL.

3. Instrument, component bench test and their integration with hardware and software are in progress.

4. The larger scale bench test, site survey, engineering design and integration with beam instrumentation are in planning.

5. Discussion on the radiation damage to the fiber optic cable.

6. Data acquisition and synchronization with beam issues.

Princeton/$\mu\mu$/00-28
K.T. McDonald
November 20, 2000
Updated January 4, 2001

Optics for E951 Target Tests in the A3 Beamline

1 Introduction

In experiment E951 [1] we will conduct studies of the interaction of intense proton pulses with liquid metal targets.

In the initial studies we plan to use a 24-GeV proton beam of up to 1.5×10^{13} per pulse, with a pulse width of about 30 ns FWHM, and a spot size of 1 mm rms radius. A candidate liquid target material is mercury, whose density ρ is 13.6 g/cm^3, and whose minimum de/dx is 1.1 MeV gm^{-1} cm^2. The density of energy deposition u due to ionization of the protons is about 33 J/gm. Additional ionization due to secondary particles from interactions of the protons in the target raises this to a peak of about 100 J/gm at 10 cm into the target, according to a MARS calculation [2], as shown in Fig 1.

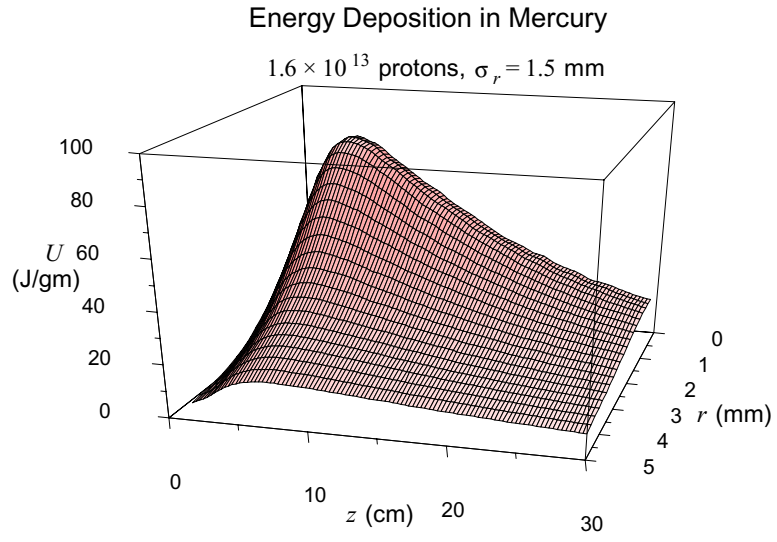

Figure 1: A MARS calculation of the profile of energy deposition by 24-GeV protons in a 30-cm-long mercury target [2].

The energy deposition u leads to pressure waves of peak stress P that can be estimated as

$$P \approx \frac{\alpha_V E_V u}{C}, \tag{1}$$

where $\alpha_V = 3\alpha$ is the volume coefficient of thermal expansion, E_V is the bulk modulus (inverse of compressibility) and C is the heat capacity per unit mass. Mercury is a candidate

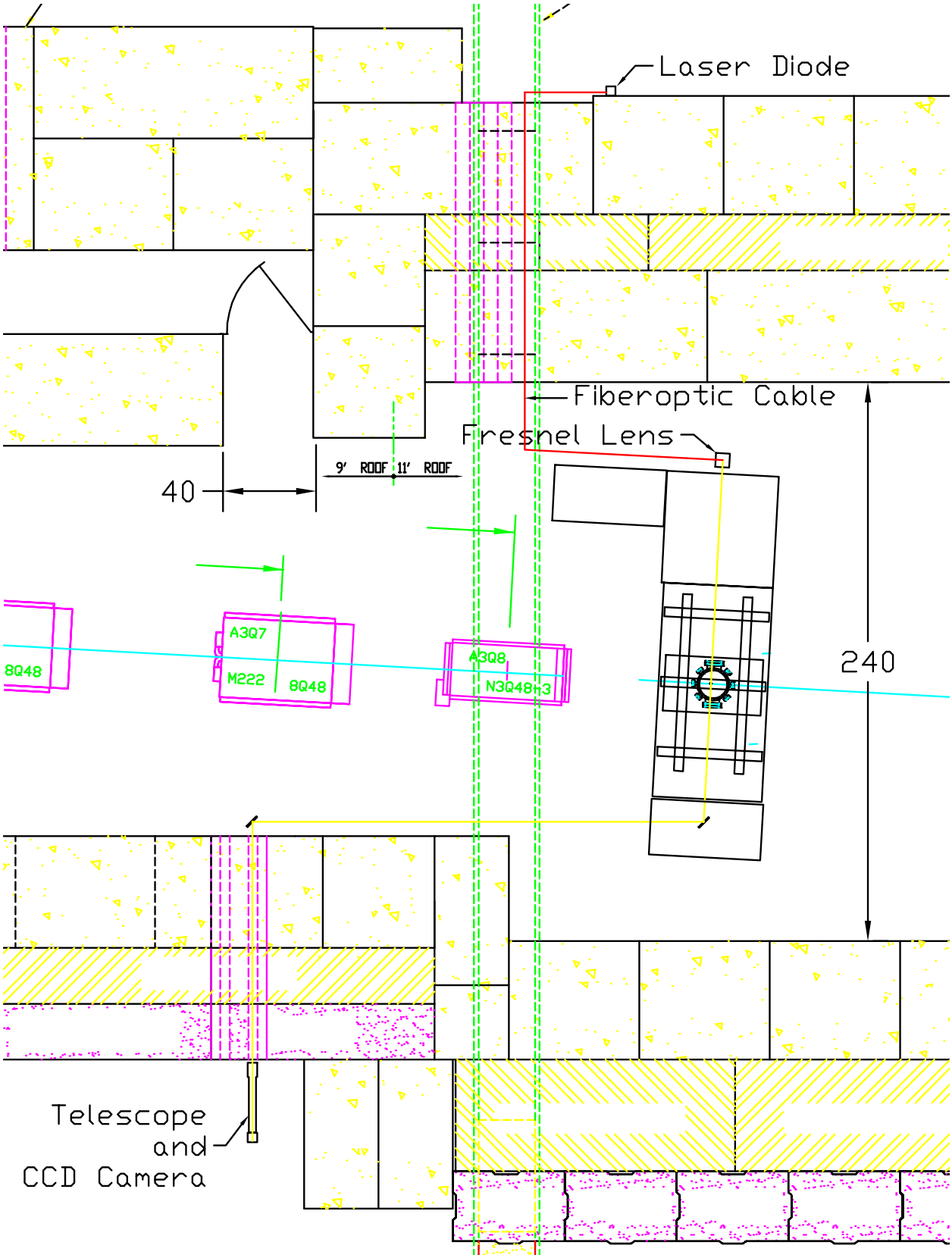

Figure 4: Layout of the optical transport between the laser diode and the high-speed camera in the A3 beamline for experiment E951.

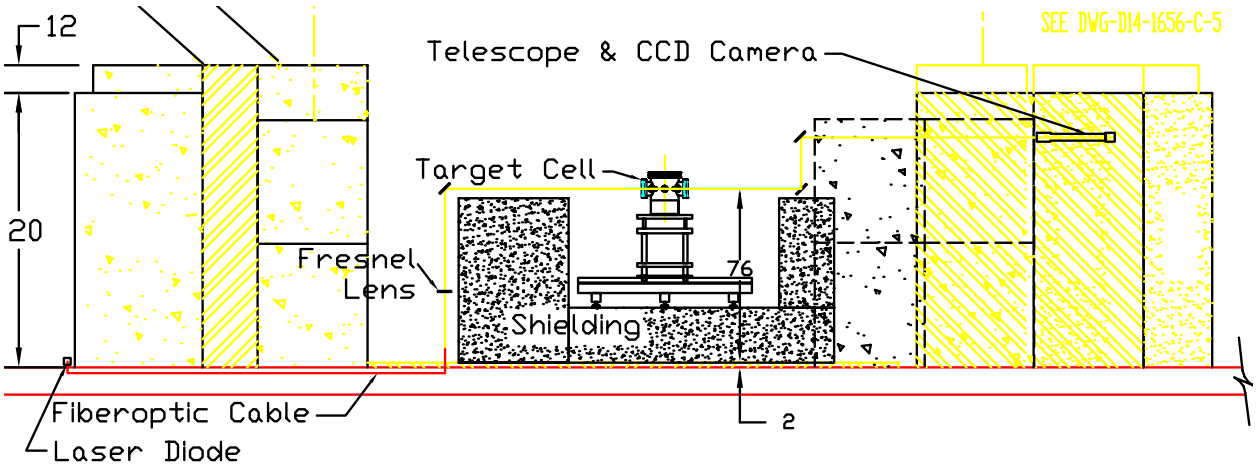

Figure 6: Elevation view of the schematic of the optical system for shadow illumination of the target in E951.

The aperture D of the field lens is then related by

$$D = A\frac{b+c}{c} = 13.75 \text{ cm} \tag{6}$$

for $A = 10$ cm and $c = 8$ m. Distance a is therefore about 0.6 m according to eq. (5).

The focal length F of the field lens is related by

$$\frac{1}{F} = \frac{1}{a} + \frac{1}{b+c}, \tag{7}$$

or $F \approx a \approx 0.6$ m $\approx 24''$, since $a \ll b + c$.

The diameter $D \approx 14$ cm of the field lens is large for a glass lens. As the quality of the field lens need not be high, it suffices to use a plastic Fresnel lens, such as available from Edmund Scientific [11]. Model NT32-691 with a $24''$ focal length and $11'' \times 11''$ area would suffice.

3 Optical Windows for the Liquid Metal Containment Vessel

The liquid metal targets to be tested in E951 will be viewed using the optical system described above through two pairs of windows, on the inner and outer containment vessels, respectively. These windows must contain any possible spray of hot liquid metal due to intense beam energy deposition, and remain reasonably transparent after the radiation dose of, say, 100 pulses of 1.6×10^{13} protons on target.

3.1 Required Impact Resistance

As discussed in the Introduction, the pressure wave induced by the proton beam energy deposition might lead to dispersal of the liquid jet into droplets of velocity $v \approx 50$ m/s (170

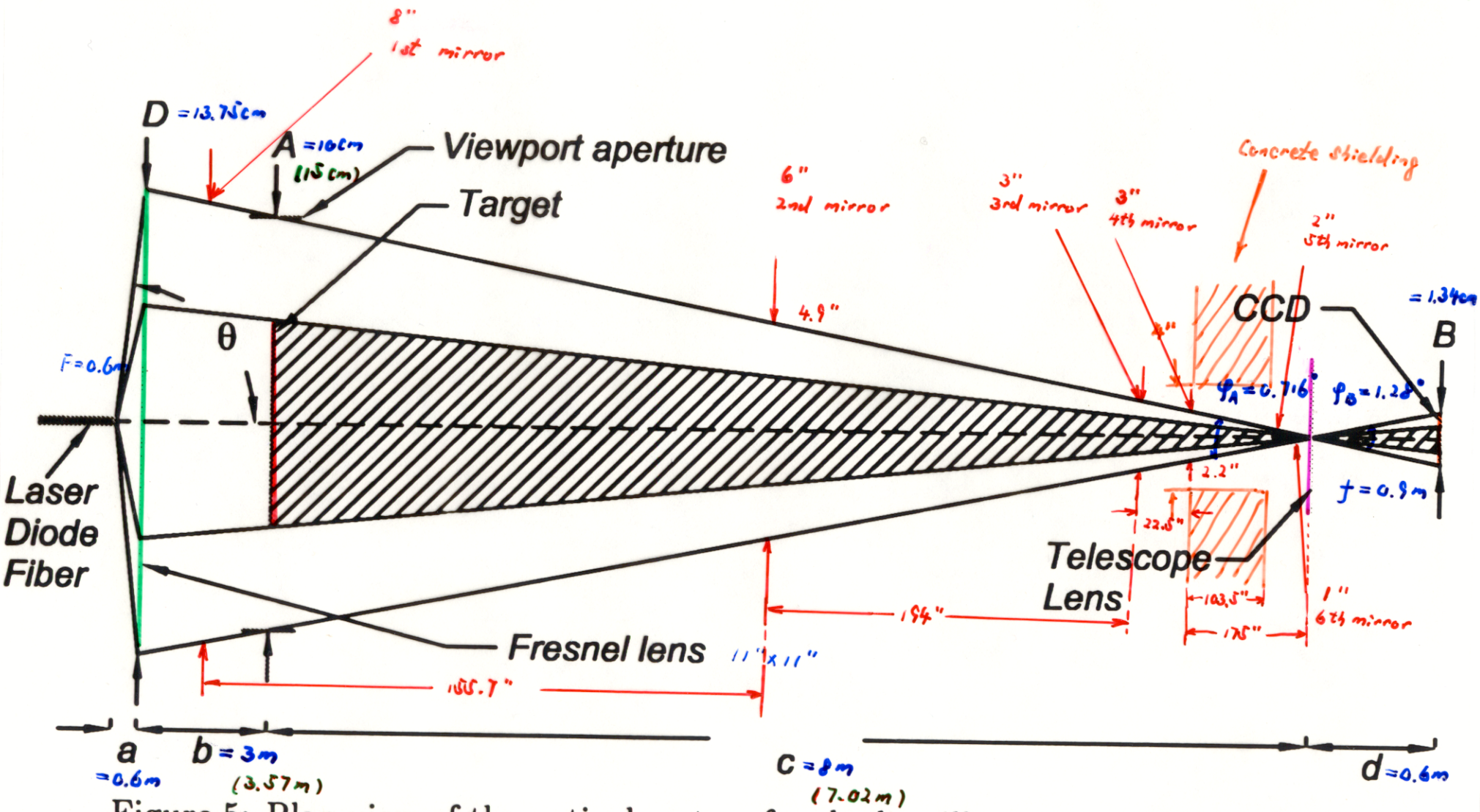

Figure 5: Plan view of the optical system for shadow illumination of the target in E951.

DALSA 64K1M

Our patented technology brings you frame rates up to 1 Million frames per second.

We've solved the problem of real-world interface to hyper-speed cameras.

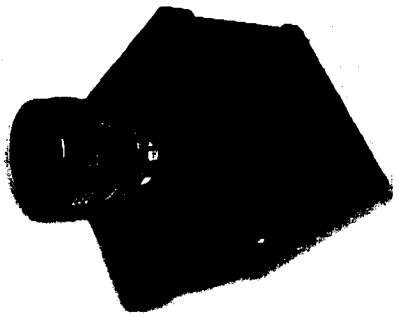

The 64K1M digital camera opens new horizons in imaging, achieving speeds of one million frames per second—and in a small, affordable package.

The custom sensor's electronic shutter allows crisp, clear images without smearing, even at maximum frame rate. True 12-bit dynamic range preserves superior image quality, even in low light conditions.

The sensor's multiple parallel channels of image data are digitized, buffered, and output through four 12-bit wide ports at 10MHz each. Maximum readout is 15 bursts per second of 17 consecutive frames.

Sensitive to UV and near IR wavelengths, the camera offers asynchronous-mode frame capture, externally triggerable to within 250 nanoseconds.

Features

- Up to one million frames per second
- High quality images
- Flexible data readout
- Extended spectral response
- Programmable operation (via RS232)

Specifications

Resolution	240 x 240
Pixel Size	56μm x 56μm
Aperture	13.4mm x 13.4mm
Lens Mount	C-mount
Max. Line/Frame Rate	Mfps (15 bursts/sec of 17 frames)
Data Rate	4x10MHz
Data Format	12-bit RS422 or LVDS
Responsivity	not available at time of printing
Dynamic Range	200:1
Nominal Gain Range	1 or 4x
Size	94x94x92mm
Mass	0.85kg
Operating Temp	0-45 C
Power Supply	+5V, -5V, +15V
Power Dissipation	30W
Regulatory Compliance	

Applications

- Ballistics
- Automotive crash testing
- Scientific research

Sensor

The 64K1M uses a custom ILT CCD. Contact SMD for more details.

Connectors

Control	SMA coax for sync
Data	2xMDR60
Power	DB15M
Other	RJ-11F for serial link

dilution factor

240 x 4 = 960 pixels

= 35 dB

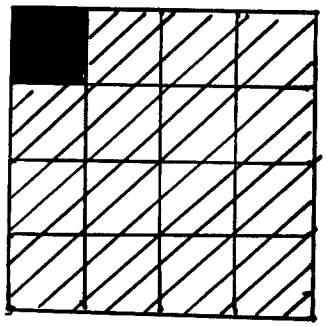

CCD 4 x 4 Pixel Array

DALSA
Technology with vision

17-Jul-00
03-70-00077-00
www.dalsa.com

Table 1: Specifications of the SMD 64K1M camera [6].

Imager	
Sensor	Custom Interline Transfer CCD
Format	240×240 pixels
Pixel size	$56\ \mu\text{m} \times 56\ \mu\text{m}$
Active area	$13.4\ \text{mm} \times 13.4\ \text{mm}$
Full Well Capacity	220 Ke^-
Fill Factor	3%
Camera Operating Parameters	
Frame Rate (max)	10^6 fps, in up to 15 bursts/sec
Sync	Internal/External
Video	12 bit RS-422 or LVDS (4 channels @ 10 MHz)
Remote RS-232 Control	Sync mode, trigger mode, electronic shutter, frame rate
Dynamic Range/Optical	
Dynamic Range	70dB
Read Noise	Less than 1.3 counts rms
Sensitivity	$8\ \mu\text{V/e}$
Dark Current	300 e/pixel per second @ 25C
Quantum Efficiency	18% max. @ 740 nm
Mechanical & Environmental	
Lens Mount	C-mount
Dimensions (W $\times$ H $\times$ L)	$3.7'' \times 3.7'' \times 4''$
Power	30 Watts
Mass	30 oz (0.85 kg)

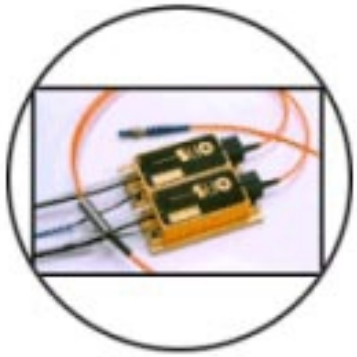

Figure 3: The 15-W, fiber-coupled, 808-nm laser diode [7].

Table 2: Specifications of the SLI 15-W, fiber-coupled, 808-nm laser diode [7].

Parameter	Min.	Typical	Max.	Unit
Power		15		W
Threshold Current	2	3	4	A
Operating Current	14	16	18	A
Numerical Aperture		0.22		
Operating Temperature		25		C
Voltage	3.6	4.0	4.2	V
Slope Efficiency	1.1	1.3	1.5	W/A
Wavelength Tolerance	± 3.0	± 5.0		nm
Connector Type		SMA 905		
Fiber Core Size		840		μm

camera is shown in Fig. 5, in which the vertical scale is expanded relative to that of the horizontal. A large Fresnel lens captures the output beam of the laser diode and focuses it through the field of view at the target onto the lens of the telescope. The CCD camera views the target through the telescope.

The distance c from the target to the telescope lens is 8 m. The aperture of the CCD sensor is $B = 0.0134$ m. The distance d from the telescope lens to the CCD is related to the

3.000e+000	–	968355
1.280e+002	–	55375
2.560e+002	–	39365
3.840e+002	–	69753
5.120e+002	–	182713
6.400e+002	–	91604
7.680e+002	–	59037
8.960e+002	–	56888
1.024e+003	–	56841
1.152e+003	–	52890
1.280e+003	–	43908
1.408e+003	–	31009
1.536e+003	–	28453
1.664e+003	–	28996
1.792e+003	–	27922
1.920e+003	–	27164
2.048e+003	–	24637
2.176e+003	–	16797
2.304e+003	–	13029
2.432e+003	–	9768
2.560e+003	–	8377
2.688e+003	–	8624
2.816e+003	–	8128
2.944e+003	–	9048
3.072e+003	–	10686
3.200e+003	–	12053
3.328e+003	–	8752
3.456e+003	–	5038
3.584e+003	–	3785
3.712e+003	–	3922
3.840e+003	–	4028
3.968e+003	–	31215

Mean: 6.47569e+002 Sigma: 9.28235e+002; Scaled Mean: 6.47569e+002 Sigma: 9.28235e+002
1997120 out of 1997120 Pixels: 100.00% of Region; Pixels 1, 1 to 1580, 1264; 0 Below Min, 0 Above Max
1 Average(s): 0.006 sec, 0, 1; Time: 2000:11:22:13: 5:36:680 End: 13: 5:36: 69 Diff: 0
SMD64K1M_10: ID # 0x0d, Rev # 0x0a, 30.0 fps, 0.006 sec, 1x1, 4x, Offset= 0, Anti-Bloom ON, HOff 12, VOff 9.

$$\text{Scroll rate} = \frac{2\,[\text{scroll}]}{6\,[\text{frame}]} * \frac{[\text{frame}]}{0.006\,[\text{sec}]} = 55.6\,\frac{[\text{scroll}]}{[\text{sec}]} \approx 60\ \text{Hz}$$

/

6ms integration time

SMD 64K-1M CCD Camera Image Capture Speed Bench Test

H. Wang, T Tsang
December 1, 2000

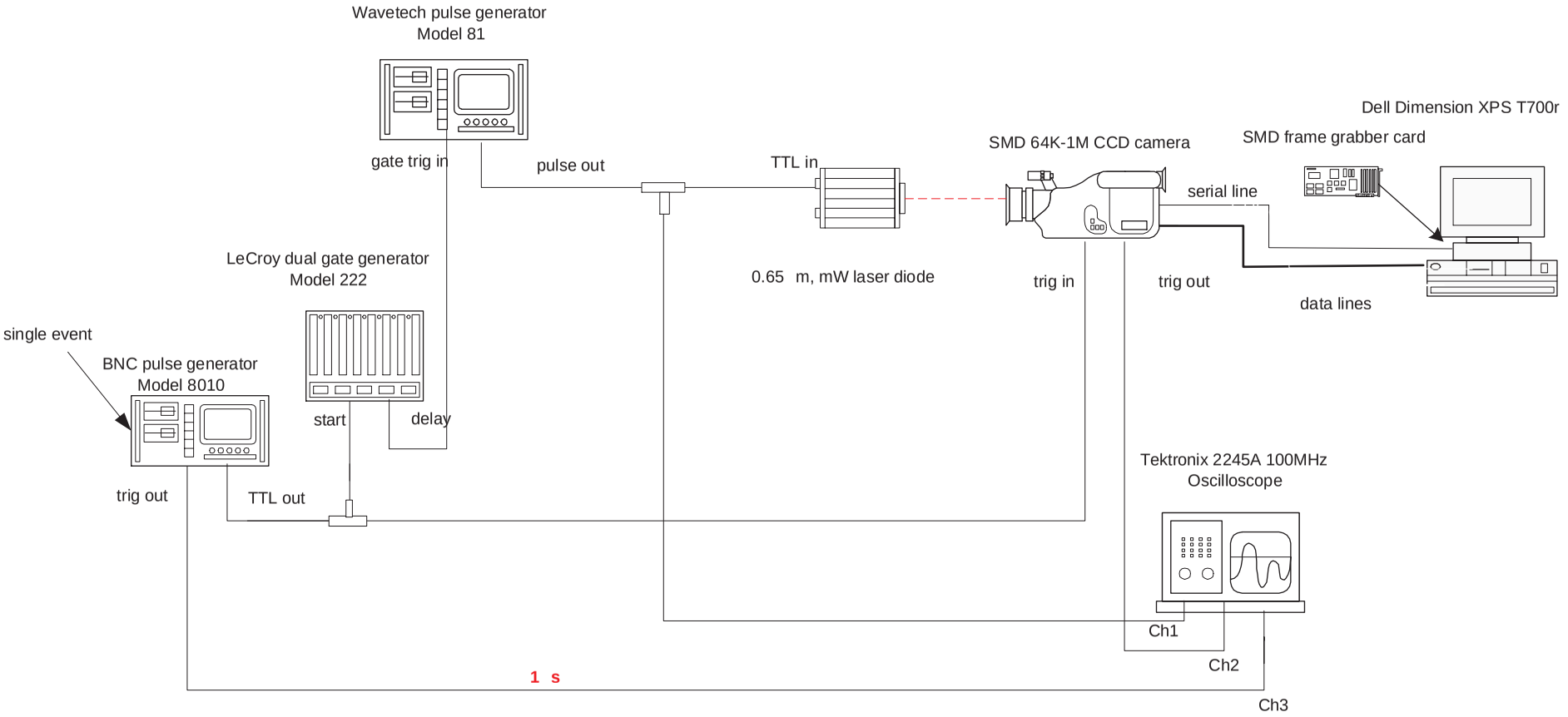

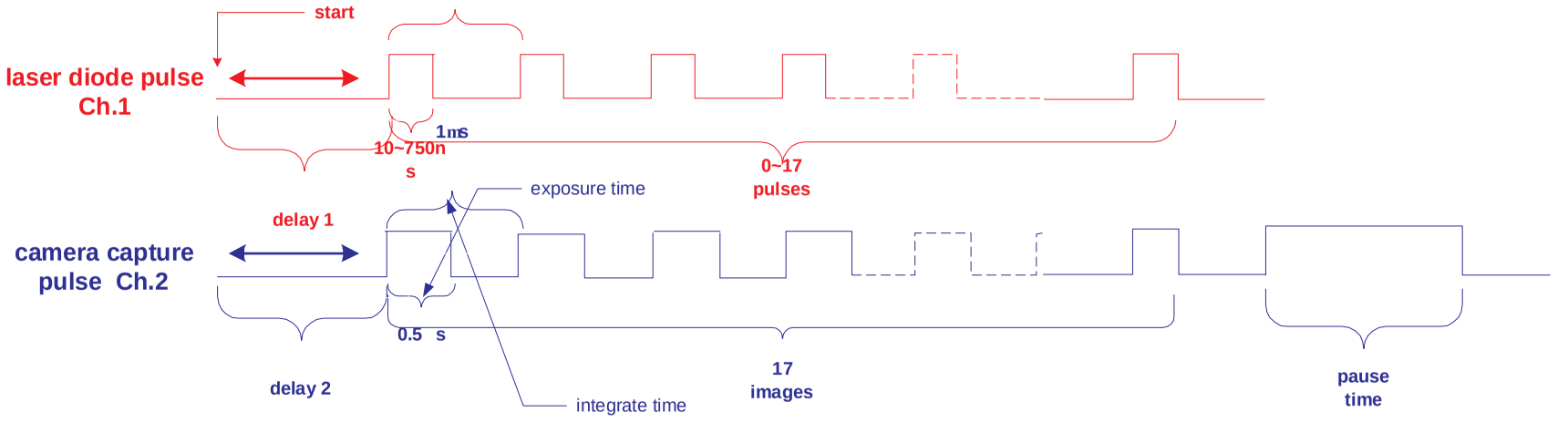

AVTECH Pulse Generator Dummy Load Test

H. Wang,
December 21, 2000

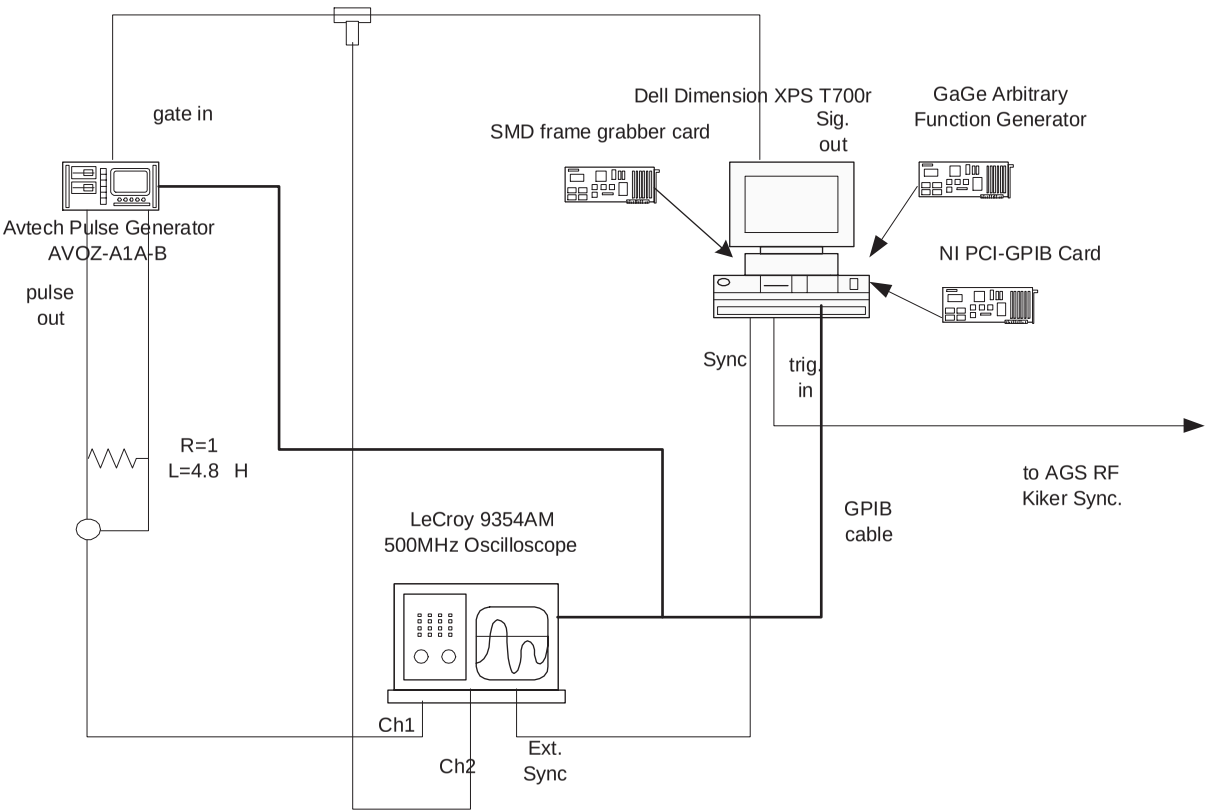

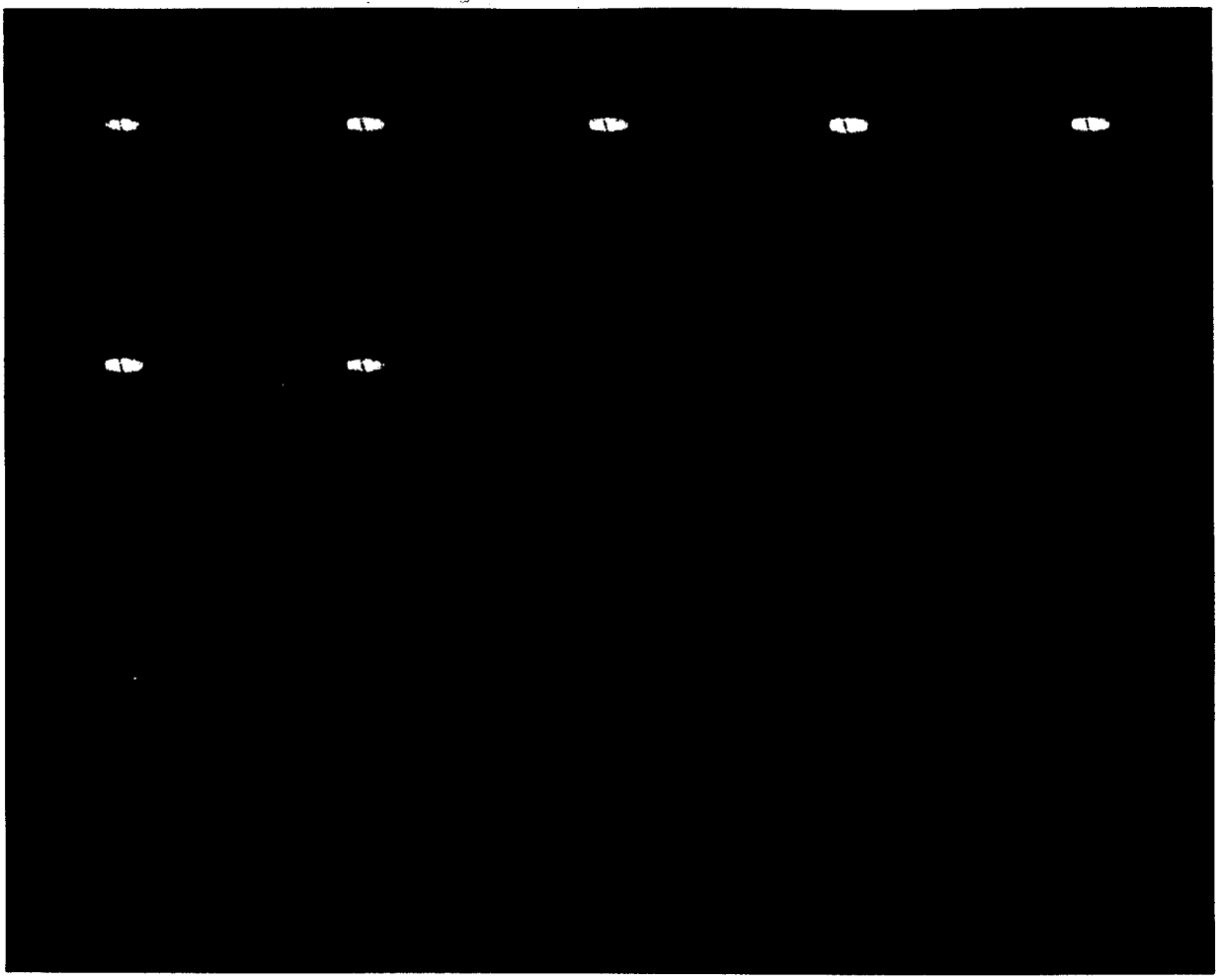

0.000e+000	–	1980408
1.280e+002	–	7451
2.560e+002	–	1759
3.840e+002	–	626
5.120e+002	–	341
6.400e+002	–	302
7.680e+002	–	273
8.960e+002	–	210
1.024e+003	–	194
1.152e+003	–	190
1.280e+003	–	192
1.408e+003	–	213
1.536e+003	–	180
1.664e+003	–	180
1.792e+003	–	179
1.920e+003	–	150
2.048e+003	–	139
2.176e+003	–	170
2.304e+003	–	135
2.432e+003	–	136
2.560e+003	–	128
2.688e+003	–	129
2.816e+003	–	136
2.944e+003	–	128
3.072e+003	–	107
3.200e+003	–	109
3.328e+003	–	131
3.456e+003	–	124
3.584e+003	–	137
3.712e+003	–	138
3.840e+003	–	114
3.968e+003	–	2311

Mean: 4.81384e+001 Sigma: 1.77408e+002; Scaled Mean: 4.81384e+001 Sigma: 1.77408e+002
1997120 out of 1997120 Pixels: 100.00% of Region; Pixels 1, 1 to 1580, 1264; 0 Below Min, 0 Above Max
R1-R2, 1 Average(s): 1e-006 sec, 0, 1; Time: 2000:11:30:10:27:41: 30 End: 10:27:41:360 Diff: 0
SMD64K1M_10: ID # 0x0d, Rev # 0x0a, 30.0 fps, 1e-006 sec, 1x1, 4x, Offset= 0, ExtInteg, Anti-Bloom ON, HOff 11, VOff 16.

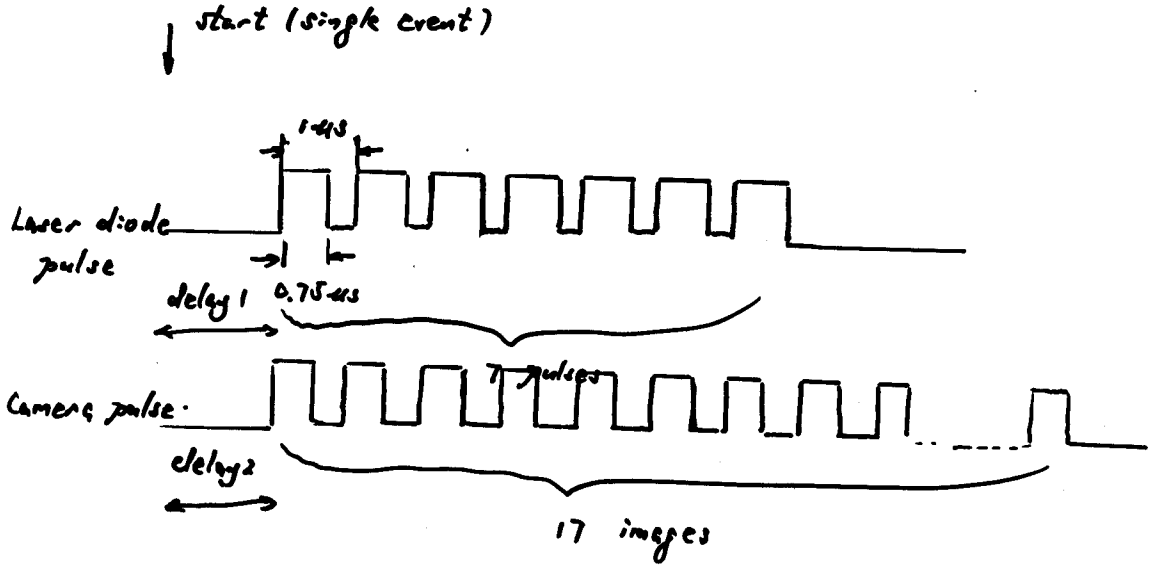

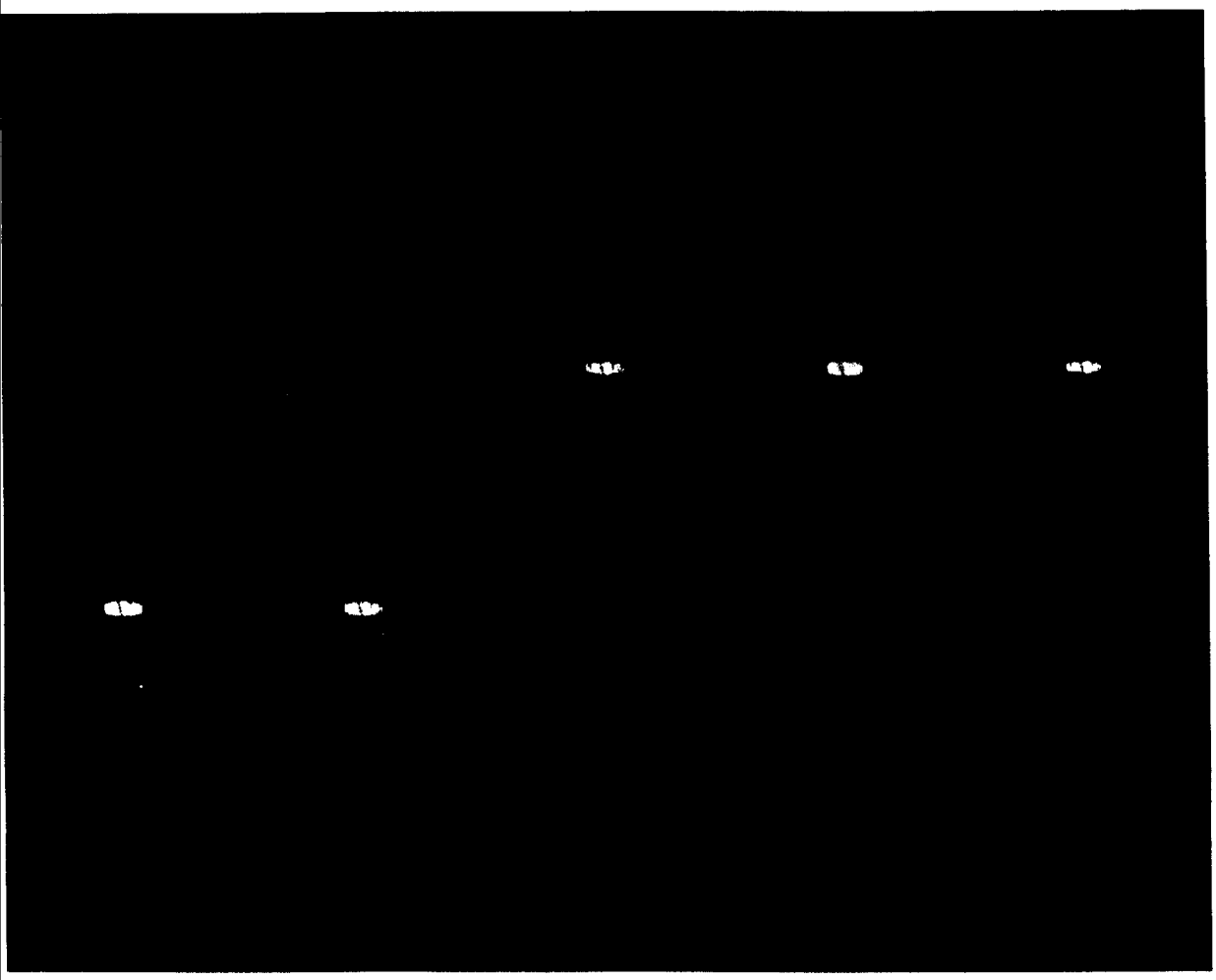

0.000e+000	–	1983965
1.280e+002	–	5900
2.560e+002	–	1615
3.840e+002	–	596
5.120e+002	–	330
6.400e+002	–	209
7.680e+002	–	165
8.960e+002	–	162
1.024e+003	–	164
1.152e+003	–	140
1.280e+003	–	130
1.408e+003	–	127
1.536e+003	–	128
1.664e+003	–	103
1.792e+003	–	128
1.920e+003	–	120
2.048e+003	–	91
2.176e+003	–	99
2.304e+003	–	115
2.432e+003	–	101
2.560e+003	–	87
2.688e+003	–	90
2.816e+003	–	89
2.944e+003	–	101
3.072e+003	–	107
3.200e+003	–	80
3.328e+003	–	82
3.456e+003	–	76
3.584e+003	–	87
3.712e+003	–	92
3.840e+003	–	104
3.968e+003	–	1737

Mean: 4.31308e+001 Sigma: 1.53409e+002; Scaled Mean: 4.31308e+001 Sigma: 1.53409e+002
1997120 out of 1997120 Pixels: 100.00% of Region; Pixels 1, 1 to 1580, 1264; 0 Below Min, 0 Above Max
R1-R2, 1 Average(s): 1e-006 sec, 0, 1; Time: 2000:11:30:10:45: 9:230 End: 10:45: 9:620 Diff: 0
SMD64K1M_10: ID # 0x0d, Rev # 0x0a, 30.0 fps, 1e-006 sec, 1x1, 4x, Offset= 0, Extinteg, Anti-Bloom ON, HOff 11, VOff 16.

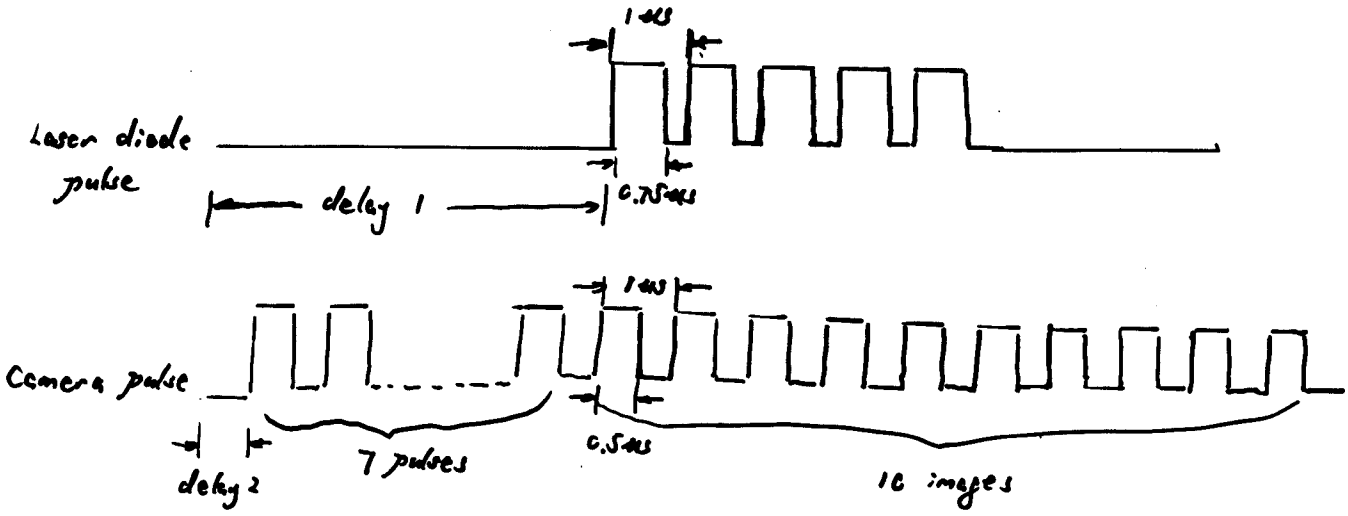

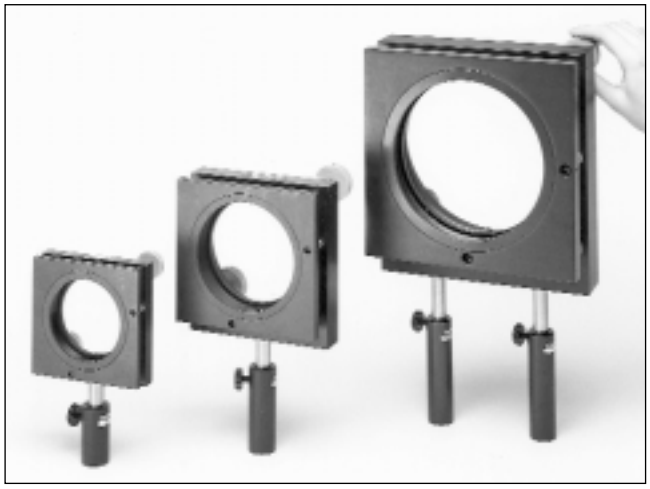

17920, 17940, and 17980 Precision Adjustable Mirror Mounts on Rods and Rod Holders.

- **High sensitivity**
- **12° range of adjustment about the vertical and horizontal axes**
- **Models for 2 to 6 inch mirrors with adapters for in between sizes**

These are our "mid-precision" mirror mounts; they offer a larger range of adjustment with higher sensitivity than the mounts described on the previous page, but aren't as sensitive as the models on the following page. The total adjustment range is ±6° (±102 mrad) about each axis. Two fine pitch thumbscrews independently control movement. The control knobs are on the back plate so your hand isn't in the beam path.

LOW DISTORTION AND STABLE ALIGNMENT

These mounts use a threaded Delrin® retaining ring to hold the mirror; the design distributes the holding force so the result is a low distortion mount. The mirror holding plate of the mount is spring loaded against a ball and the rounded ends of the two adjustment screws, providing stable, wobble free motion.

ADAPTERS FOR SMALLER DIAMETER OPTICS

The adapters listed on the previous page to hold "in-between" sized optics and Helium Neon laser heads also work with these mirror mounts.

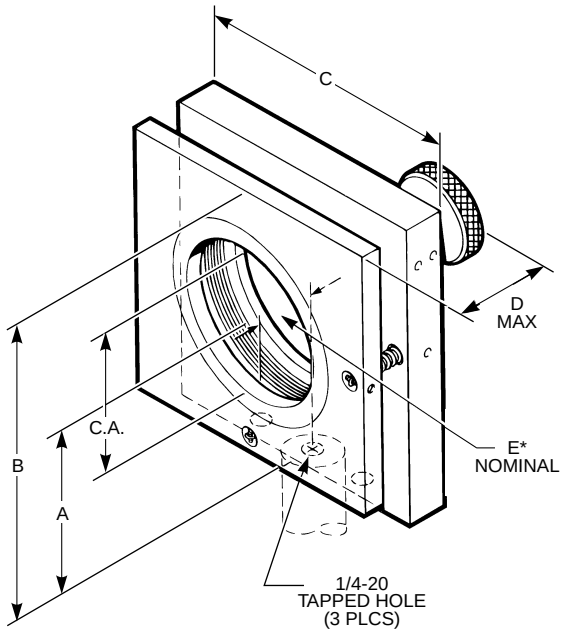

MODEL	DIMENSIONS IN INCHES (mm)					
	A	B	C	D	E*	C.A.
17920	2.0 (50.8)	3.68 (93.5)	3.38 (86)	1.7 (43.2)	0.7 (17.8)	1.75 (44.5)
17940	2.25 (57.2)	4.25 (108)	4.25 (108)	2.0 (50.8)	0.83 (21.1)	2.75 (70)
17960	3.25 (82.6)	5.75 (146.1)	5.5 (140)	3.3 (83.8)	1.87 (47.5)	3.75 (95.3)
17980	5.0 (127)	8.75 (222.3)	8.0 (203.2)	4.5 (114.3)	2.4 (61)	5.75 (146.1)

* "E" is the nominal distance from the rod axis to the center of the front face of the mirror.

Dimensions in inches (mm)

Fig. 1 Dimensional diagram of Precision Adjustable Mirror Mounts.

MOUNTING

These mirror mounts have tapped 1/4-20 holes in the bottom. They are most commonly rod mounted. Use magnetic rod holders for freedom of movement.

For the 4 and 6 Inch Mounts, we recommend that you use large optical rods or a base, for stability. Mounting bases increase the optical centerline by 0.5 inch (12.7 mm).

SPECIFICATIONS AND ORDERING INFORMATION

Precision Adjustable Mirror Mounts

Mirror Diameter inch (mm)	Mirror Thickness Range inch (mm)	Clear Aperture inch (mm)	Total Range of Adustment degrees (mrad)	Sensitivity arc s (µrad)	Model No.	Price
2.0 (50)	0.13 to 0.5 (3.3 to 13)	1.75 (44)	12 (204)	0.8 (4)	**17920**	
3.0 (76)	0.13 to 0.75 (3.3 to 19)	2.8 (71)	12 (204)	0.6 (3)	**17940**	
4.0 (102)	0.13 to 1.0 (3.3 to 25)	3.8 (96)	12 (204)	0.4 (2)	**17960**	
6.0 (152)	0.38 to 1.5 (9.6 to 38)	5.75 (146)	12 (204)	0.2 (1)	**17980**	

Mounting Bases

For Mount	Model No.	Price
17920/17940	**17892**	
17960	**17894**	
17980	**17896**	

AOM110 Series Manual Gimbal Mount Dimensions

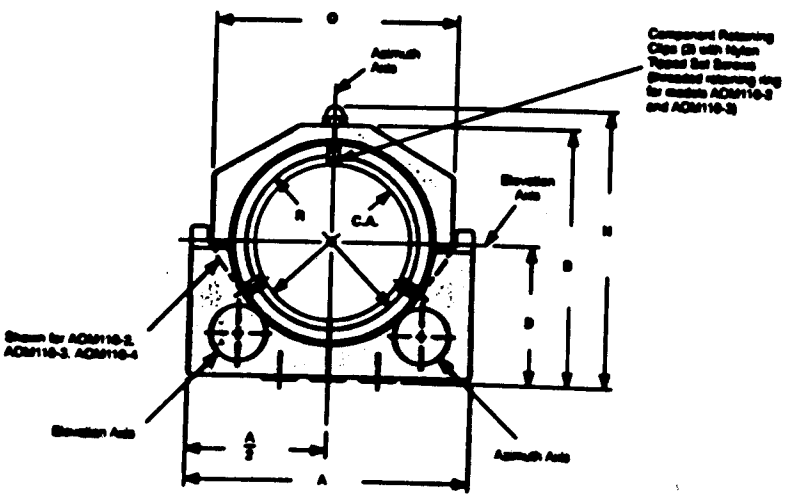

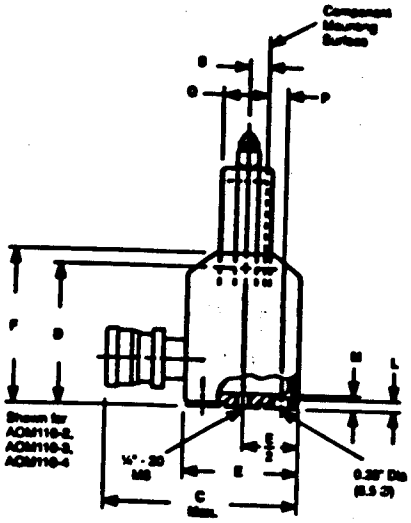

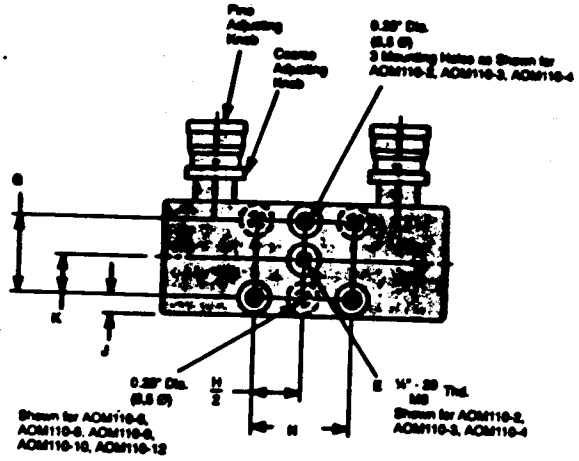

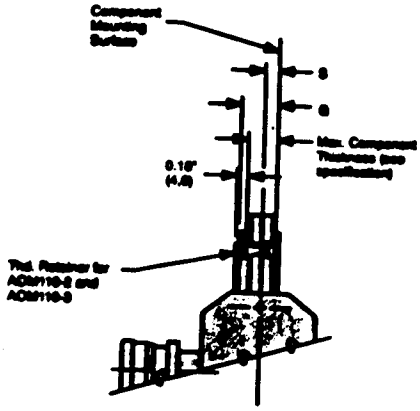

	A	B	C	D	E	F	G	H	J	K	L	M	N	O	P	Q	R	S	C.A.
AOM110-2	4.00" (101.6)	3.53" (89.7)	3.44" (87.4)	2.00" (50.8)	1.88" (47.6)	2.19" (55.7)	1.00" (25.0)	2.00" (50.0)	0.50" (14.9)	0.44" (11.0)	0.09" (2.3)	0.25" (6.4)	—	3.25" (82.6)	0.20" (4.9)	0.62" (15.8)	2.04" (51.9)	0.24" (6.1)	1.82" (46.3)
AOM110-3	5.00" (127.0)	4.47" (113.6)	3.50" (88.9)	2.44" (62.0)	2.00" (50.8)	2.62" (66.6)	1.00" (25.0)	2.00" (50.0)	0.56" (14.5)	0.44" (11.0)	0.09" (2.3)	0.31" (7.9)	—	4.25" (108.0)	0.19" (4.7)	0.70" (17.8)	3.06" (77.7)	0.26" (6.6)	2.77" (70.4)
AOM110-4	6.25" (158.8)	5.95" (151.2)	4.06" (103.2)	3.19" (81.1)	2.50" (63.5)	3.44" (87.4)	2.00" (50.0)	2.00" (50.0)	0.25" (6.8)	1.00" (25.0)	0.09" (2.3)	0.31" (7.9)	—	5.44" (138.2)	0.62" (15.4)	0.75" (19.1)	4.06" (103.2)	0.38" (9.7)	3.75" (95.3)
AOM110-6	9.00" (228.6)	8.62" (219.0)	4.78" (121.4)	4.56" (115.8)	3.00" (76.2)	4.94" (125.5)	2.80" (69.8)	4.00" (100.0)	0.50" (13.1)	—	0.35" (8.9)	0.38" (9.7)	9.00" (228.6)	8.00" (203.2)	0.50" (12.3)	1.18" (30.0)	6.06" (154.0)	0.50" (12.7)	5.69" (144.6)
AOM110-8	12.25" (311.2)	11.87" (301.5)	5.19" (131.9)	6.31" (160.3)	3.50" (8.09)	6.81" (17.03)	2.00" (50.0)	6.00" (150.0)	0.75" (19.5)	—	0.41" (10.5)	0.50" (12.7)	12.40" (315.0)	11.13" (282.7)	0.38" (9.3)	1.50" (40.4)	8.09" (205.5)	0.62" (15.7)	7.63" (193.9)
AOM110-9	13.50" (342.9)	13.12" (333.3)	5.44" (138.2)	6.94" (176.3)	3.75" (95.3)	7.75" (196.9)	2.00" (50.0)	6.00" (150.0)	0.88" (22.7)	—	0.47" (12.0)	0.50" (12.8)	13.65" (346.8)	12.38" (314.5)	0.25" (6.4)	1.63" (41.5)	9.09" (230.9)	0.75" (19.1)	8.62" (219.0)
AOM110-10	14.75" (374.7)	14.25" (362.0)	5.69" (144.6)	7.50" (190.5)	4.00" (101.7)	8.13" (206.5)	2.00" (50.0)	6.00" (150.0)	1.00" (25.8)	—	0.47" (12.0)	0.50" (12.8)	14.78" (375.5)	13.50" (343.0)	0.00" (0.5)	2.12" (53.9)	10.12" (257.1)	1.00" (25.4)	9.62" (244.4)
AOM110-12	16.00" (667.2)	17.50" (444.9)	6.06" (154.0)	9.25" (235.0)	4.50" (114.4)	9.75" (247.7)	3.00" (75.0)	10.00" (250.0)	0.75" (19.7)	—	0.59" (15.0)	0.63" (16.0)	18.33" (465.8)	16.50" (419.2)	0.56" (13.7)	2.12" (53.9)	12.12" (307.9)	0.96" (23.9)	11.99" (292.2)

Note: For metric mounting holes and grid pattern add "M" suffix. e.g. AOM110-6M.

AVTECH AVOZ-A1A-B Dummy Load Pulse Test

H. Wang, Jan. 05, 2001

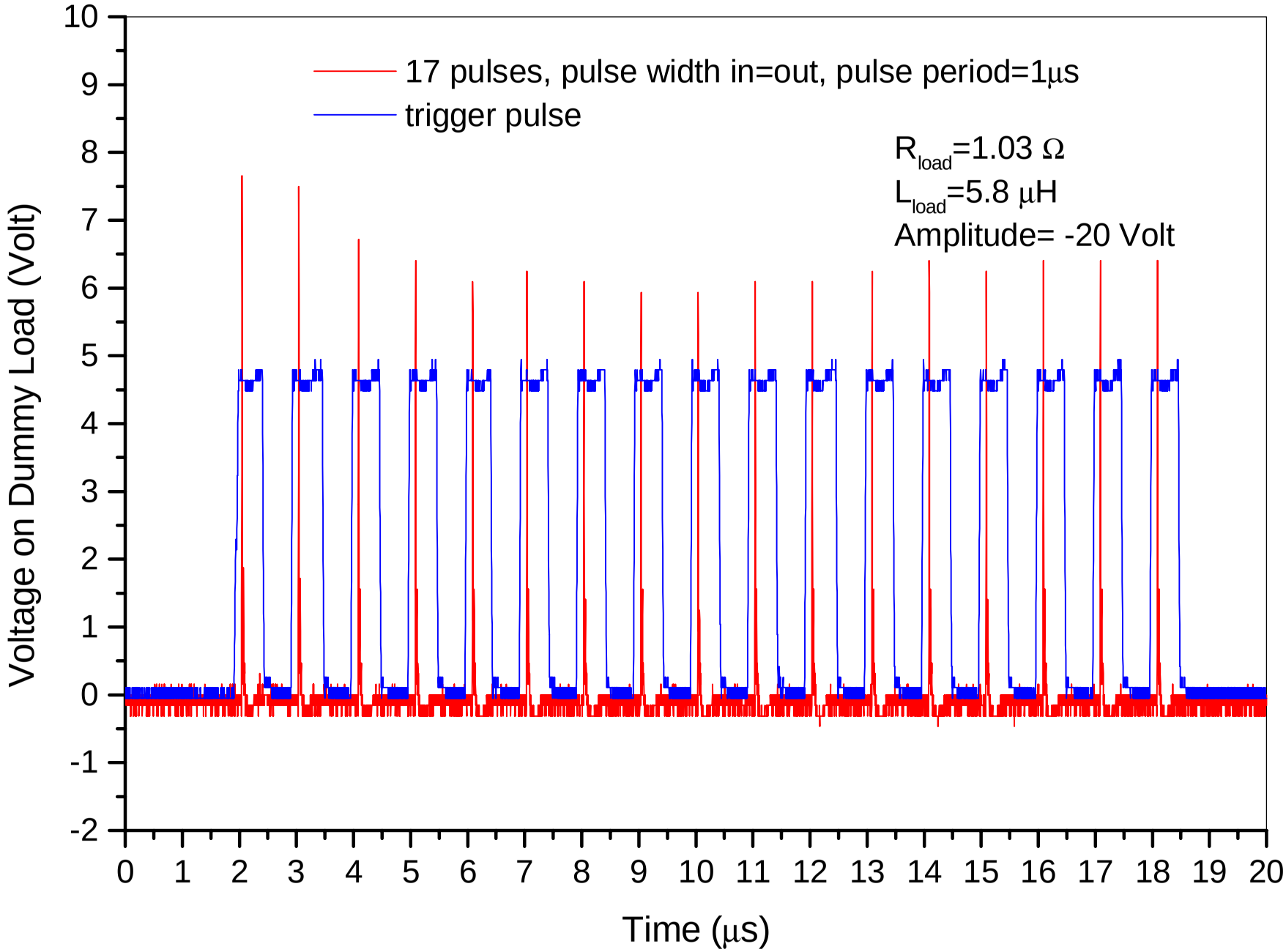

AVTECH AVOZ-A1A-B Dummy Load Pulse Test

H. Wang, Dec. 21, 2000

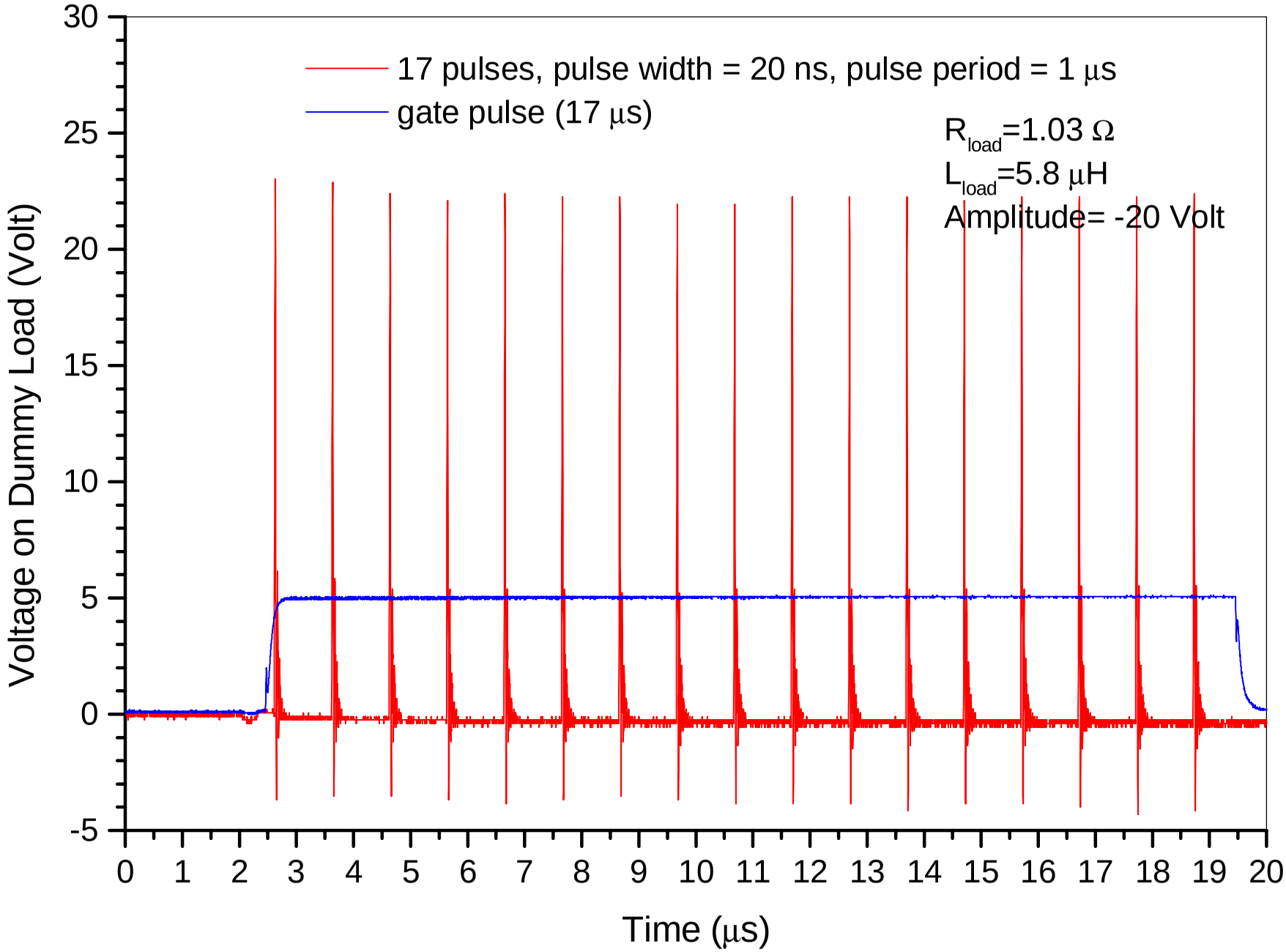

AVTECH AVOZ-A1A-B Dummy Load Pulse Test

H. Wang, Jan. 05, 2001

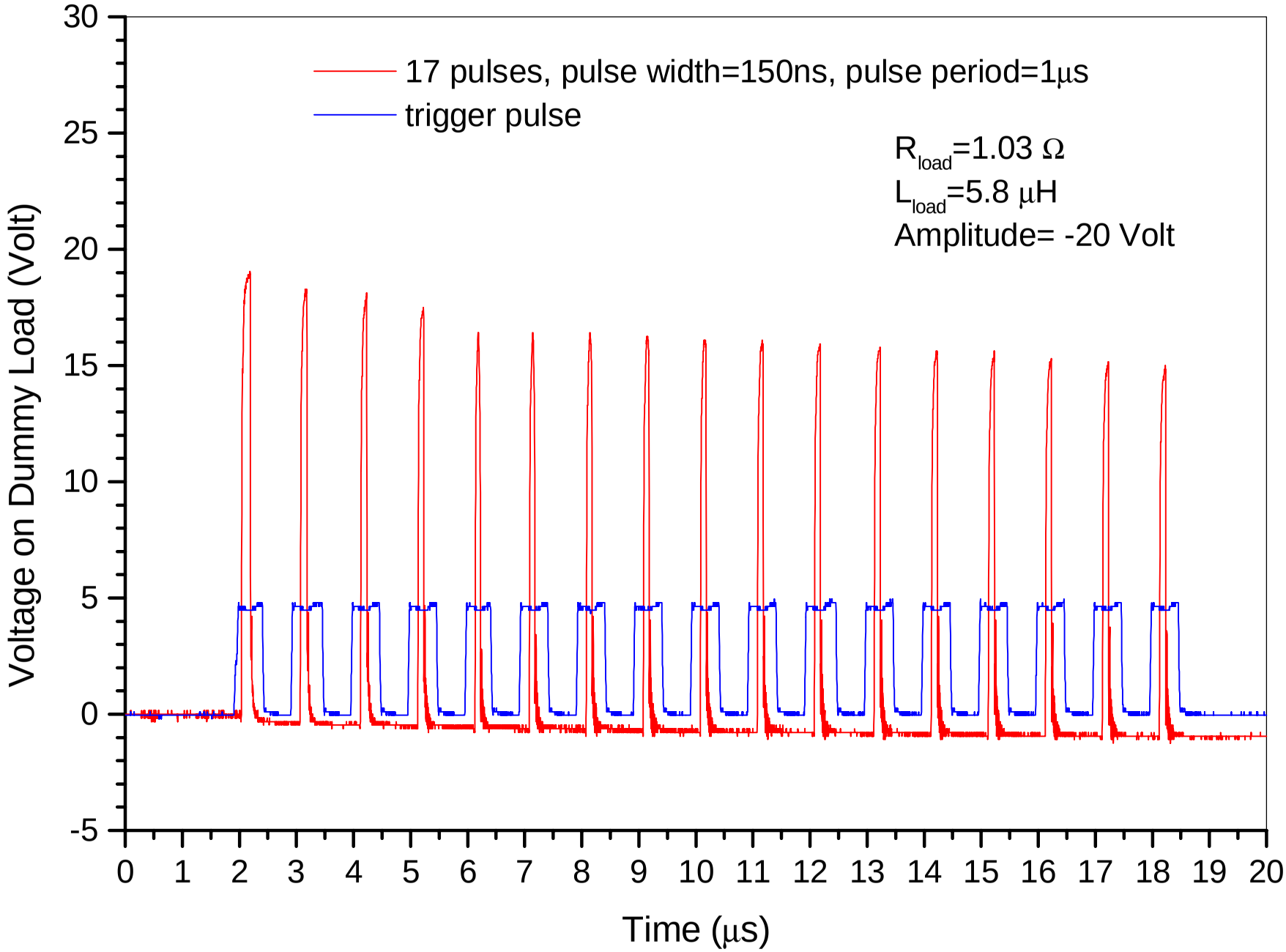

Radiation Effects on Fiber Optic Cable Studied by NASA:

http://epims.gsfc.nasa.gov/tva/meldoc/cabass/

Much study has been made of the effects of ionizing radiation, both Gamma and from source natural to the space flight environment, on optical fiber. Information can be found in the literature documenting the dependency of a fiber's performance in a radiation environment on the materials used to make the glass, the processes used, coatings used, dose type and rate and total dose. Recovery times, self-annealing and photobleaching effects have also been well documented. Manufacturers interested in the space flight market are aware of these dependencies and have developed manufacturing processes which produce products which can withstand tens to hundreds of kRads(Si) total dose with less than one dB increase in loss per kilometer of fiber. Flight projects using multimode fiber, use lengths much shorter than a kilometer and have tended to consider radiation sensitivity a non-issue. With the emergence of the use of single mode fiber, the radiation issue is being revisited to examine the compatibility of the recovery times (³ 2 sec) with the high data rates being applied.

Optical fiber will darken due to ionizing radiation creating centers of absorption where unwanted elements and other optical defects occur in the fiber. Generally a fiber will experience defects during the drawing process making them hard to isolate and eliminate, regardless of the purity of the glass pre-form. Radiation performance can also be affected by the coatings. There is evidence that suggests that the primary coating on the fiber has a much greater impact on the radiation performance of a fiber than does the secondary coating. Polyimide coatings undergo a heat cure while acrylates undergo a ultraviolet (UV) cure. It has been surmised that the high temperature cure inherent in the polyimide coating process can actually anneal the defects induced in the fiber by the drawing process. [4]

Germanium, used to dope fiber cores in order to raise the waveguide index of refraction, causes radiation sensitivity. Phosphorous doped fiber (for the core or cladding) has been well documented as not acceptable for use in space environments due to its radiation sensitivity[5]. Lower temperatures produce the largest radiation induced attenuation in fibers. The radiation induced loss sensitivity can vary by a factor of 25 between temperature extremes where the worst case is at the low end of the temperature range. At lower temperatures the annealing of color centers decreases. In general it is best to use pure silica in space applications when total dose requirements exceed 5kRads(Si) [6].

Dose rate will have an effect on the results of radiation testing when they are above 960 rads(Si)/hour [6,7]. Often bit error rate has been used as a pass/fail criterion making dose rate dependence much less obvious. When attenuation is measured, special attention should be given to dose rate and kept as low as feasible Test data has been generated for many fibers with a variety of material formulations to total dose levels through and beyond 1 MRads(Si) [6]. An algorithm has been established by NRL which allows extrapolation of radiation performance data for varying values of total dose, temperature, and dose rate [8].

References:

4. C. E. Barnes, R. A. Greenwell, G. W. Nelson., "The effect of fiber coating on the radiation response of fluorosilicate clad, pure silica core step index fibers," SPIE proceedings Vol. 787 1987.

5. E. J. Friebele, "Survivability of Photonic Systems in Space" DoD Fiber Optics Conference, McLean VA, March 24-27, 1992.

6. E. J. Friebele, "Photonics in the Space Environment," IEEE Nuclear Space Radiation Effects Conference, San Diego CA, 1991.

7. Akira Iino, Junich Tamura, "Radiation Resistivity in Silica Optical Fibers", Journal of Lightwave Technology, Vol. 6(2), pp. 145-149, IEEE 1988.

8. E. J. Friebele, M.E. Gingerich, D. L. Griscom, "Extrapolating Radiation-Induced Loss Measurements in Optical Fibers from the Laboratory to Real World Environments", 4th Biennial Department of Defense Fiber Optics and Photonics Conference, March 22-24, 1994.

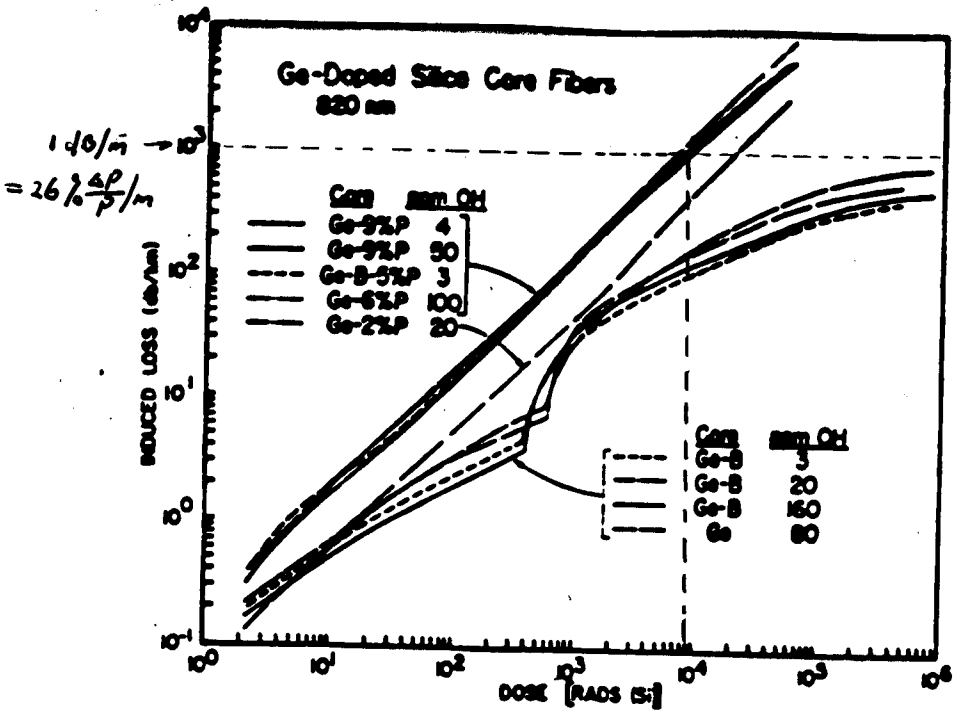

Fig. 2. Growth of radiation-induced-attenuation at 0.82 μm in Ge-doped silica core fibers either undoped or codoped with B and/or P during steady-state irradiation.

From "Compositional effects on the Radiation Response of Ge-doped Silica-core Optical Fiber Waveguides"
E. Friebele etc.
Applied Optics
Vol. 19, No. 17, Sep. 1, 1980

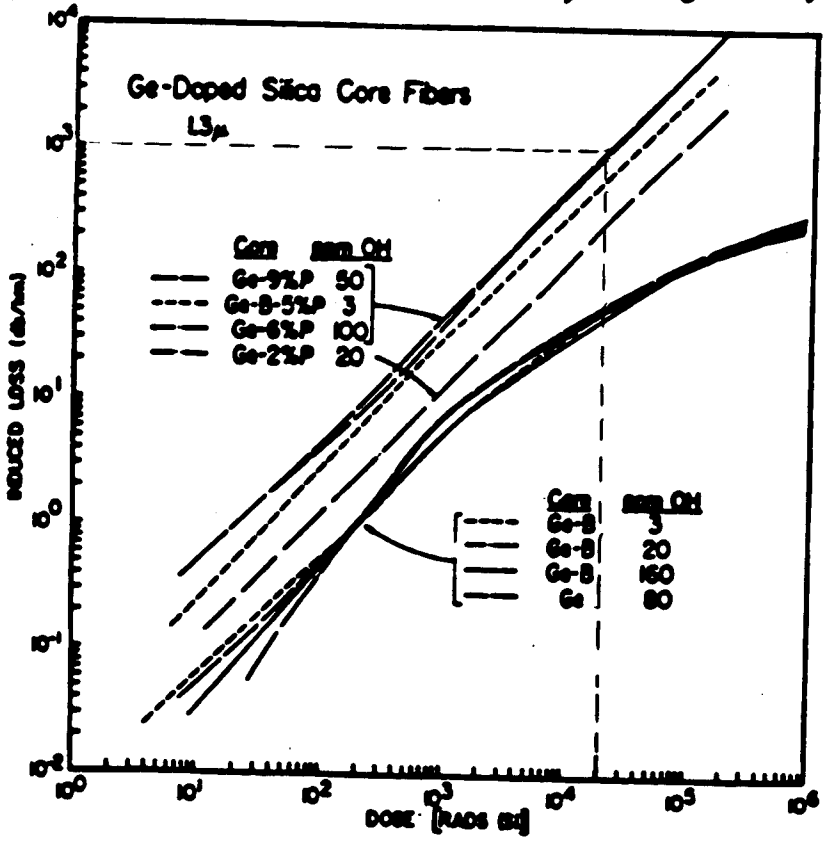

Fig. 3. Growth of radiation-induced attenuation at 1.3 μm in Ge-doped silica-core fibers during steady-state irradiation. Note the decreased radiation response of these fibers at 1.3 μm *vis à vis* 0.82 μm (Fig. 2).

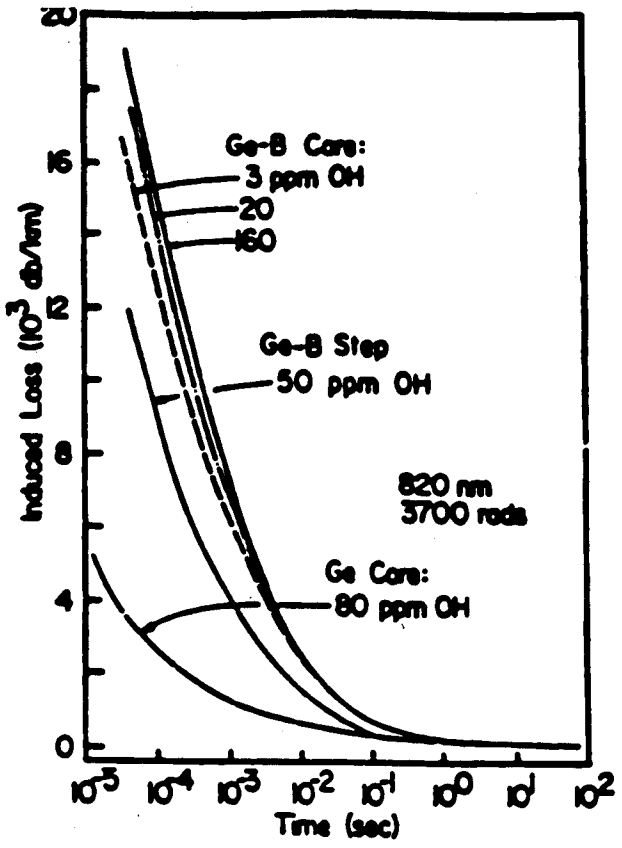

(a)

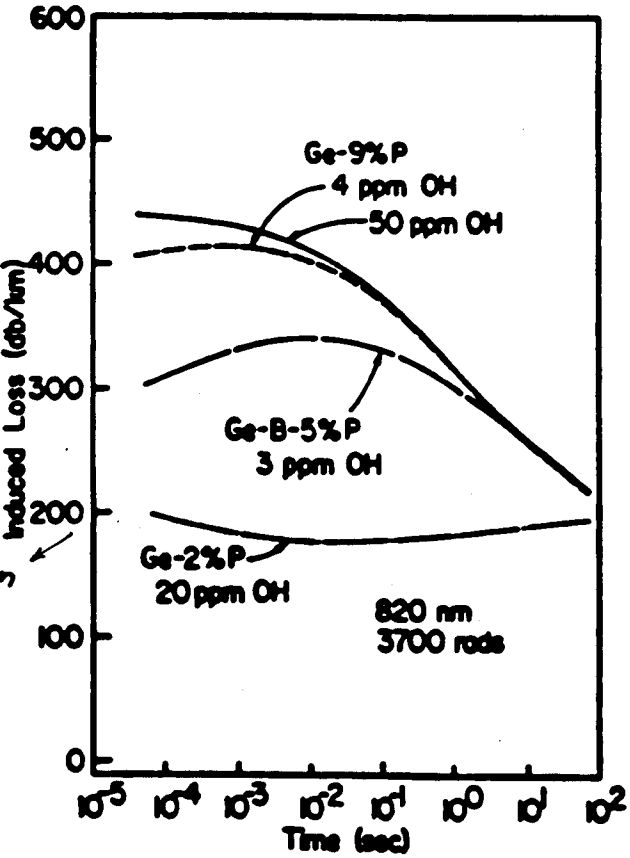

0.2 dB/m
$= 5\% \frac{\Delta P}{P}/m$

(b)

Fig. 4. Time evolution of the radiation-induced attenuation at 0.82 μm in (a) Ge–B-doped silica and Ge-doped silica and (b) Ge–P-doped silica and Ge–B–P-doped silica-core optical fibers following a 3-nsec 3700-rad pulsed electron irradiation. Dose rate = 1.2×10^{12} rad/sec.

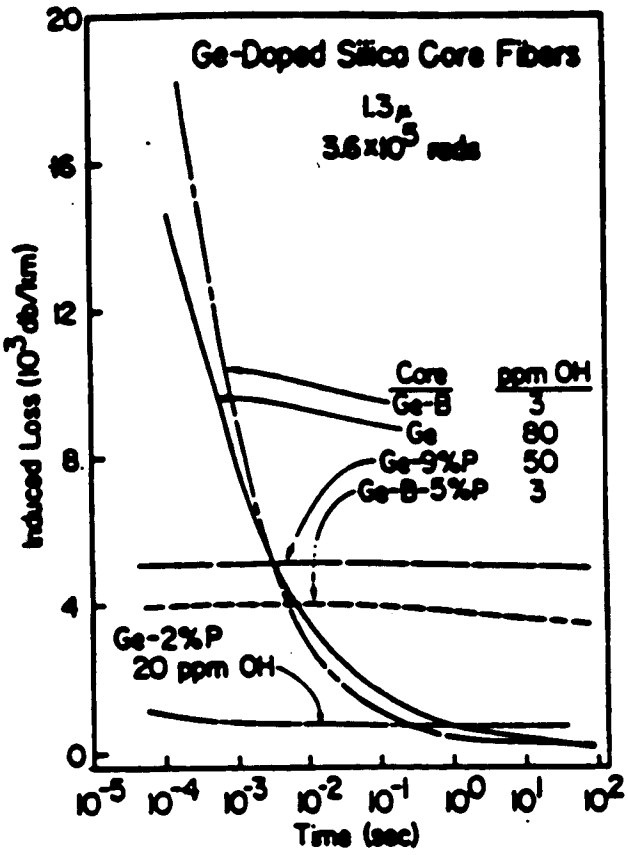

ig. 5. Time evolution of the radiation-induced attenuation of Ge-oped silica-core fibers at 1.3 μm following a pulsed electron irradiation of 360,000 rad. Dose rate = 1.2×10^{14} rad/sec; T = 300 K.

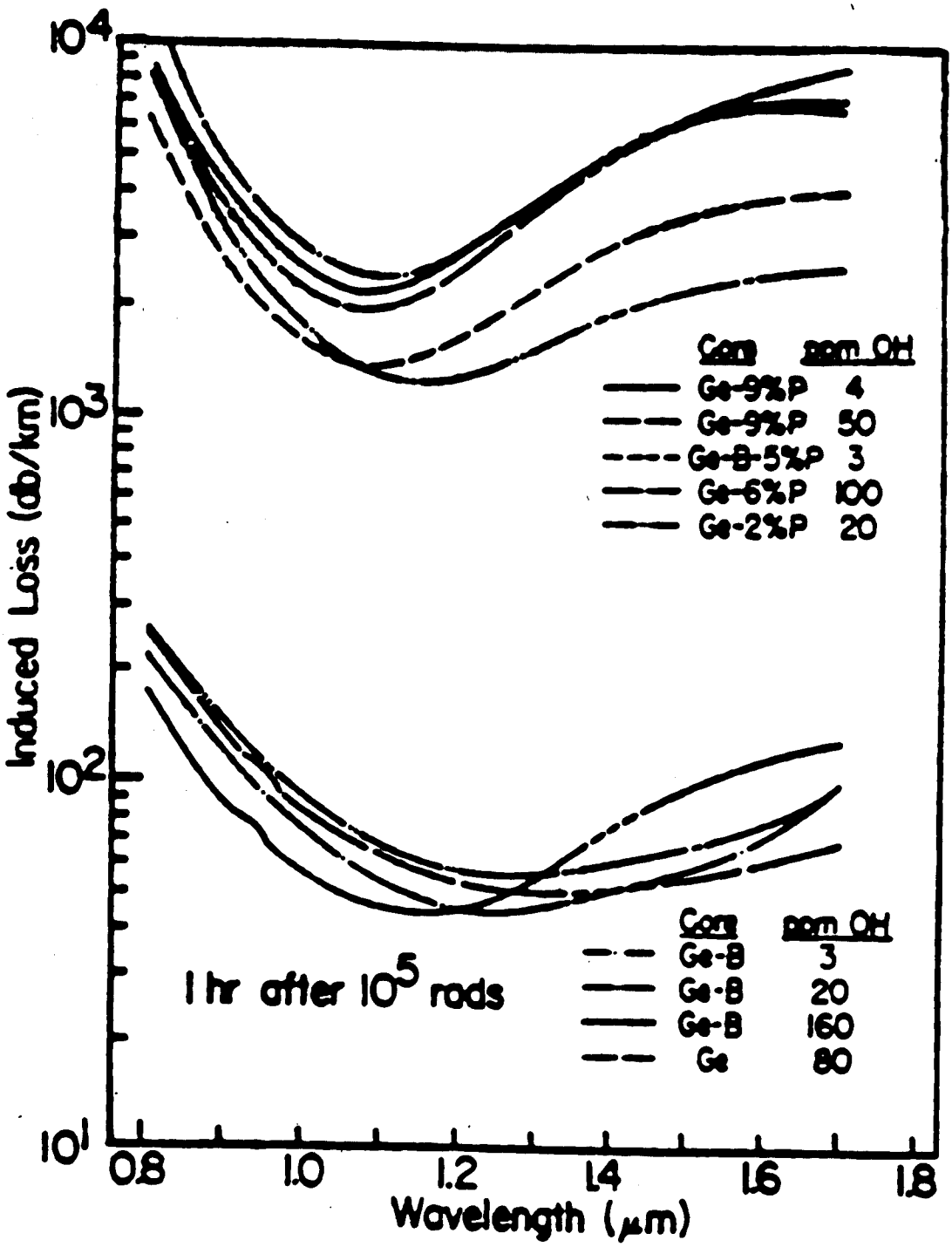

duced absorption of Ge-doped silica-core optical waveg
.67) was used to strip the cladding modes. Short dashe
cond OH overtone band at 1.37 μm made determination
although such changes could have been easily detected i
d at 1.37 μm could be used with confidence in fibers wi

BNL E951 Experiment High Speed Camera System Work Plan

Color Code:
red: done
blue: in progress
green: near plan
Magenta: far plan
gold: goal
red larrow line: optic related relationship